Low-Rank and Sparse Matrix Decomposition for Compressed Sensing Reconstruction of Magnetic Resonance 4D Phase Contrast Blood Flow Imaging (LoSDeCoS 4D-PCI)

Jana Hutter[1,2], Peter Schmitt[4], Gunhild Aandal[3], Andreas Greiser[4], Christoph Forman[1,2] , Robert Grimm[1], Joachim Hornegger[1,2], and Andreas Maier[1,2]

[1] Pattern Recognition Lab, University Erlangen-Nuremberg, Germany
[2] School of Advanced Optical Technologies, Erlangen, Germany
[3] University Hospital Cleveland, Cleveland, Ohio, USA
[4] Siemens AG Healthcare Sector, Magnetic Resonance, Erlangen, Germany

Abstract. Blood flow measurements using 4D Phase Contrast blood flow imaging (PCI) provide an excellent fully non-invasive technique to assess the hemodynamics clinically in-vivo. Iterative reconstruction techniques combined with parallel MRI have been proposed to reduce the data acquisition time, which is the biggest drawback of 4D PCI. The novel LoSDeCoS technique combines these ideas with the separation into a low-rank and a sparse component. The high-dimensionality of the PC data renders it ideally suited for this approach. The proposed method is not limited to a single body region, but can be applied to any 4D flow measurement. The benefits of the new method are twofold: It allows to significantly accelerate the acquisition; and generates additional images highlighting temporal and directional flow changes. Reduction in acquisition time improves patient comfort and can be used to achieve better temporal or spatial resolution, which in turn allows more precise calculations of clinically important quantitative numbers such as flow rates or the wall shear stress. With LoSDeCoS, acceleration factors of 6-8 were achieved for 16 in-vivo datasets of both the carotid artery (6 datasets) and the aorta (10 datasets), while decreasing the Normalized Root Mean Square Error by over 10 % compared to a standard iterative reconstruction and by achieving similarity values of over 0.93. Inflow-Outflow phantom experiments showed good parabolic profiles and an excellent mass conservation.

1 Introduction

Knowledge about patient-specific hemodynamics is important in the diagnosis and treatment planning of various cardiovascular diseases such as stenoses or aneurysms in the carotid arteries or in the aorta. Dynamic 3D flow information allows to visualize not only the flow rate, but also turbulent flow as well as the hemodynamics in complex or pathologic vessel systems. Standard clinically used

K. Mori et al. (Eds.): MICCAI 2013, Part I, LNCS 8149, pp. 558–565, 2013.

techniques including Doppler ultrasound or Digital Substraction Angiography have the drawbacks of user-dependent results or the exposure to ionizing radiation. 4D PCI provides a fully non-invasive alternative to assess three-directional blood flow. The acquisition time for this technique, especially if high temporal and spatial resolution or an extended anatomic coverage are desired, tends to be very high, limiting its wider clinical use at present. With recently proposed combinations of compressed sensing algorithms and parallel MRI techniques using data simultaneously acquired by multiple coils, significant reductions of the acquisition time were achieved.

1.1 PCI Acquisition

The data for an MR volume is acquired by successive k-space scans until the full k-space $\mathbf{Y}$ is covered. Reconstruction using the matrix $\mathbf{A}$ leads to the final volume $\mathbf{X} = \mathbf{AY}$ with $\mathbf{Y} \in \mathbb{C}^{N_k}$ and $\mathbf{X} \in \mathbb{C}^N$ with $N = N_x \times N_y \times N_z$. The traditional reconstruction is done by simple inverse Fourier Transform $\mathbf{A} = \mathbf{F^{-1}}$.

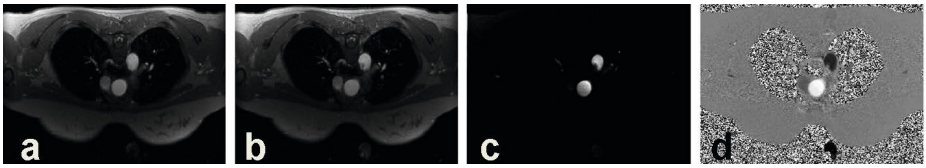

Fig. 1. Aortic Phase Contrast dataset: (a) Flow compensated image, (b) Magnitude of velocity sensitive image, (c) Phase Contrast image and (d) Phase Difference image

The technique typically uses ECG triggering to acquire N_p phases in the cardiac cycle. As the data is collected over multiple heart cycles until k-space coverage is complete, reduction of the number of required k-space lines leads to a direct decrease in acquisition time. To visualize the flow dynamics in three directions, four MR scans are needed: one velocity-compensated scan $\mathbf{Y_{v0}}$; and three scans sensitive to the velocity $\mathbf{Y_{v1}}, \mathbf{Y_{v2}}$ and $\mathbf{Y_{v3}}$ [1] (see Fig. 1a,b). For a final series of images with N_p temporal phases which are sensitive to flow in three directions, $4N_p$ full 3D datasets have to be acquired and reconstructed from the same spatial field of view. Combining all three encodings leads to the typical PCI image: $\mathbf{PC} = \sum (\mathbf{X_{v0}} - \mathbf{X_{vs}})^2$. (Fig. 1c) The velocity information is obtained by calculating the phase difference between the velocity compensated and each of the velocity encoded scans: $\Delta_s = \arg(\mathbf{X_{v0}}) - \arg(\mathbf{X_{vs}})$ (Fig. 1d).

1.2 Spatial Redundancy

Compressed sensing algorithms rely on sampling only $\bar{N_k} << N_k$ k-space samples. In order to achieve good image quality with data sampled below the Nyquist criteria, dedicated reconstruction techniques are required, which rely

on prior knowledge as regularization. Commonly used regularization terms include Wavelet Transforms, Total Variation or temporal smoothness.

The 4D flow dataset contains a high degree of anatomical redundancy between the $4N_p$ different volumes, as they are all acquired from the same spatial region. Particularly important for this acquisition technique are the flow changes across the different temporal phases, appearing in a small fraction of the volume. The final volume can thus be split into a shared anatomical- structural part and the regions with directionally and spatially varying flow characteristics. This separation agrees well with a mathematical separation into a low-rank and a sparse component. The reconstruction of the images (zoom to the ICA/ECA) using 48/5/2 singular values (Fig. 2) shows well the separation possibilities. The image quality concerning the vascular structures and the surrounding tissue is preserved with less singular values, while the temporal and spatial flow variations over time are lost.

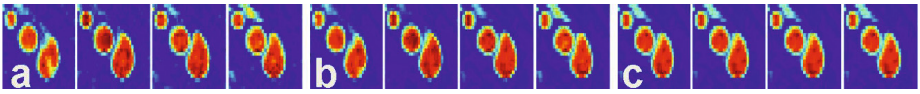

Fig. 2. Reconstruction with (a) 48, (b) 5 and (c) 2 singular values

1.3 State of the Art

Iterative reconstruction algorithms have been recently applied to PCI using different regularizations and algorithms [2,3,4]. Employed algorithms include Lagrangian based alternating direction [5] and Split Bregman, successfully applied to MRI by Aeltermann et al. [6]. Splitting the problem into a sparse and a low-rank part was discussed by Candès et al.[7] and recently introduced for brain, multi-slice breast and dynamic MRI [8,9,10]. The novel LoSDeCoS algorithm exploits the special properties of 4D Phase Contrast data for the division into a low-rank and sparse component and solves for that using a specially adapted Split Bregman solver able to deal with Total Variation, L_1 and the nuclear norm.

2 Iterative Reconstruction Using LoSDeCoS

Each volume $\mathbf{X}$ is transformed into a vector $\boldsymbol{x}$ containing all image pixels. This allows to significantly enlarge the vector space used for low-rank estimation. All 4D flow volumes, both the temporal phases and the velocity encodings are used to form a common matrix $\mathbf{M} \in \mathbb{C}^{N \times 4N_p}$.

$$\mathbf{M} = \begin{bmatrix} \boldsymbol{x}_0^{v0,0} & \boldsymbol{x}_0^{v1,0} & \boldsymbol{x}_0^{v2,0} & \boldsymbol{x}_0^{v3,0} & \cdots & \boldsymbol{x}_0^{v0,N_p} & \boldsymbol{x}_0^{v1,N_p} & \boldsymbol{x}_0^{v2,N_p} & \boldsymbol{x}_0^{v3,N_p} \\ \vdots & \vdots & \vdots & \vdots & \cdots & \vdots & \vdots & \vdots & \vdots \\ \boldsymbol{x}_N^{v0,0} & \boldsymbol{x}_N^{v1,0} & \boldsymbol{x}_N^{v2,0} & \boldsymbol{x}_N^{v3,0} & \cdots & \boldsymbol{x}_N^{v0,N_p} & \boldsymbol{x}_N^{v1,N_p} & \boldsymbol{x}_N^{v2,N_p} & \boldsymbol{x}_N^{v3,N_p} \end{bmatrix} \quad (1)$$

2.1 Division into a Low-Rank and a Sparse Matrix

$\mathbf{M}$ consists of a low rank part $\mathbf{L}$, representing stationary tissue, and a sparse matrix $\mathbf{S}$ of the same dimensions. The sparse part includes the highly varying but sparse regions, which contain moving magnetization (flow).

The low rank requirement $\text{rank}(\mathbf{L}) < r$ is due to computational efforts relaxed to the convex nuclear norm $||\mathbf{L}||_* = \sum \omega$, where ω are the singular values of $\mathbf{S}$, as calculated by the complex SVD. The sparse component should fulfill $||\Phi S||_{L_0} < c$, with Φ being an operator that transforms the data into a sparse domain. The LoSDeCoS method uses both Wavelet (Ψ) and isotropic TV norm as sparsifying transforms. The calculated minimization therefore equals to $\min_{\mathbf{S}} \alpha_1 ||\mathbf{S}||_{TV} + \alpha_2 ||\psi \mathbf{S}||_{L_1}$.

2.2 Iterative Reconstruction with the Split Bregman Algorithm

The parallel MRI reconstruction algorithm requires coil profiles $\mathbf{C_c}$ describing the sensitivity information of the N_c spatially varying coils. Those profiles, the discrete Fourier transform $\mathbf{F}$ as well as the undersampling projection $\mathbf{P}$ form the iterative reconstruction matrix $\mathbf{A} = \mathbf{PFC}$, which is used to fit the calculated image $\mathbf{M}$ to the acquired undersampled data $\mathbf{y}$ by minimizing the data fidelity term $||\mathbf{AM} - \mathbf{y}||^2_{L_2}$. The final objective function used in the minimization problem reads as follows:

$$\min_{\mathbf{S},\mathbf{L}} ||\mathbf{A}(\mathbf{S}+\mathbf{L}) - \mathbf{y}||^2_{L_2} + \alpha_1 ||\mathbf{S}||_{TV} + \alpha_2 ||\psi \mathbf{S}||_{L_1} + \alpha_3 ||\mathbf{L}||_* . \tag{2}$$

The combination of different norms makes the problem hard to solve in the form of an unconstrained minimization problem (2). The Split Bregman algorithm is better suited, as it splits the problem into its different components, which are then minimized each with an adapted strategy. Additional variables $\mathbf{d}_\nabla = (\nabla \mathbf{S})$, $d_w = \psi \mathbf{S}$, $d_n = \mathbf{L}$ and the residual errors $\boldsymbol{\mu}$ are used to combine the actual solutions of all steps in a common L_2 minimization step. The algorithm is initialized with $\mathbf{S} = \mathbf{L} = 0$ as well as $\boldsymbol{\mu} = 0$ (residual variables) and consists of three substeps in every iteration.

$$\begin{cases} (\mathbf{S}^{k+1}, \mathbf{L}^{k+1}) = & \text{argmin}_{\mathbf{S}^k, \mathbf{L}^k} \left|\left|\mathbf{A}(\mathbf{L}^k + \mathbf{S}^k) - \mathbf{y}\right|\right|^2_{L_2} + \alpha_3 \left|\left|d_n^k - \mathbf{L}^k - \mu_n^k\right|\right|^2_{L_2} \\ & + \alpha_1 \left|\left|\mathbf{d}_\nabla{}^k - \nabla \mathbf{S}^k - \mu_\nabla{}^k\right|\right|^2_{L_2} + \alpha_2 \left|\left|d_w^k - \psi \mathbf{S}^k - \mu_w^k\right|\right|^2_{L_2} & \text{(3a)} \\ (\mathbf{d}_\nabla{}^{k+1}) = & \text{argmin}_{\mathbf{d}_\nabla{}^k} \left|\left|\mathbf{d}_\nabla{}^k - \nabla \mathbf{S}^{k+1} - \mu_\nabla^k\right|\right|^2_{L_2} + \left|\left|\nabla \mathbf{S}^{k+1}\right|\right|_{2,1} & \text{(3b)} \\ (d_w^{k+1}) = & \text{argmin}_{d_w} \left|\left|d_w^k - \psi \mathbf{S}^{k+1} - \mu_w^k\right|\right|^2_{L_2} + \left|\left|\psi d_w^k\right|\right|_{L_1} & \text{(3c)} \\ (d_n^{k+1}) = & \text{argmin}_{d_n^k} \left|\left|d_n^k - \mathbf{L}^{k+1} - \mu_n^k\right|\right|^2_{L_2} + \left|\left|d_n^k\right|\right|_* & \text{(3d)} \end{cases}$$

First, the L_2 problem (3a) is minimized using a limited-memory Quasi-Newton algorithm with three iterations. The obtained results $\mathbf{S}^{k+1}, \mathbf{L}^{k+1}$ are used in the next step, which successively minimizes the regularization terms using adapted methods for each of them: The isotropic TV (3b) was minimized using adapted shrinkage [11], Wavelet (3c) with soft thresholding. The nuclear norm minimization is done with singular value thresholding. The complex SVD for $\mathbf{L}$ results in

$\mathbf{L} = \mathbf{U}\Sigma\mathbf{V}^*$. The nuclear norm is equal to $\sum tr(\Sigma)$. The new $\mathbf{L}$ is computed as $\mathbf{L}^{k+1} = \mathbf{U}\bar{\Sigma}\mathbf{V}^*$ with $\bar{\Sigma} = diag(\bar{\sigma_{i,i}})|\bar{\sigma_{i,i}} = \sigma_{i,i}$ if $\sigma_{i,i} \geq \epsilon_n$ and $\bar{\sigma_{i,i}} = 0$ if $\sigma_{i,i} \leq \epsilon_n$. ϵ_n is chosen fixed for all datasets as $0.1\sigma_{i,i}$.

The last step is the update of the residual variables μ as follows: ${\mu_\nabla}^{k+1} = {\mu_\nabla}^k + \nabla\mathbf{S}^{k+1} - {\mathbf{d}_\nabla}^{k+1}$, $\mu_w^{k+1} = \mu_w^k + \psi\mathbf{S}^{k+1} - d_w^{k+1}$and $\mu_n^{k+1} = \mu_n^k + \mathbf{L}^{k+1} - d_n^{k+1}$.

3 Experiments and Results

3.1 Experimental Setup

Volunteer data (10 aortic datasets, 6 carotid datasets) was acquired on a clinical 3T scanner (MAGNETOM Skyra, Siemens Healthcare, Erlangen). In addition, phantom data was acquired using an MR compatible pump (CompuFlow 1000, Shelley). Further evaluation was done on the phantom data. The inflow-outflow setup used for this study with two connected tubes of diameter 1.9mm and a regulated parabolic flow with 150 ml/s allows to study quantitative values such as the flow and the conservation of mass. The parameters for the carotid/aortic/phantom data were TR 49.8/41.9/49.6 ms, TE 3.5/2.7/3.4 ms, flip angle 20 ° and slice thickness 4/5/3.1mm. The FOV was 200×200×40mm for carotids (matrix 256^2), 340×230×25mm for the aorta (matrix 416×288) and 190×130mm for the phantom (matrix 176×256). Temporal phases and velocity sensitivity range (venc) were chosen patient specific, between 10 and 16 phases and venc $\in [60, 150]$cm/s.

The whole k-space was acquired for all datasets and retrospectively undersampled using sampling patterns $\mathbf{U}$ incoherent in both temporal phase and velocity encoding direction. An acceleration factor of 8, corresponding to 32 lines out of 256 was applied to the carotid datasets and the phantom data. For the aortic data the acceleration factor was 6. The fully sampled directly reconstructed data $\mathbf{X}_{REF}$ is used for evaluation purposes. The undersampled data was reconstructed three times. Using an iterative SENSE approach without regularization $\mathbf{X}_{IS}$, a compressed sensing SENSE approach involving both TV and L_1 regularization $\mathbf{X}_{IRS}$ and with the proposed novel LoSDeCoS method $\mathbf{X}_{LOS}$. The parameters were chosen identical for all datasets as $\alpha_1 = 0.00005, \alpha_2 = 0.005, \alpha_3 = 0.05$, ten LBFGS iterations and six outer iterations.

3.2 Quantitative Evaluation

The normalized root mean square error $NRMSE(\mathbf{R}, \mathbf{X}) = ||\mathbf{R} - \mathbf{X}||_2^2 \,/\, ||\mathbf{X}||_2^2$, as well as the structured similarity measure SSIM [12] were used to evaluate the LoSDeCoS results against the reference and the standard reconstruction methods. To assess the image quality, angiography specific Contrast-to-Noise-Ratios (CNR) were used.

$$\mathrm{SSIM}(\mathbf{R}, \mathbf{X}) = \frac{2\mu_\mathbf{R}\mu_\mathbf{X} + c_1}{\mu_\mathbf{X}^2 + \mu_\mathbf{R}^2 + c_1} + \frac{\sigma\sigma_{\mathbf{XR}} + c_2}{\sigma_\mathbf{R}^2 + \sigma_\mathbf{X}^2 + c_2} \mathrm{CNR}(\mathbf{X}) = \frac{\mu_{\mathbf{X_{T1}}} - \mu_{\mathbf{X_{T2}}}}{\sqrt{0.5(\sigma^2_{\mathbf{X_{T1}}} + \sigma^2_{\mathbf{X_{T2}}})}}. \quad (4)$$

For the phantom data, the deviation from mass conservation, involving total inflow F_i and outflow F_o was evaluated: $DM = |F_i - F_o| / F_i$ (0 in ideal settings).

4 Results

The upper row of Fig. 3 shows the results for the fully sampled reference against different reconstruction results using the same acceleration of 8. The influence of separating low-rank and sparse components is illustrated in the lower row of Fig. 3 showing the $\mathbf{L}, \mathbf{S}$ and $\mathbf{M}$ for the temporal phases $t_1 = 100\,ms$, and $t_2 = 250\,ms$. Especially the filling of the internal carotid artery is well visualized in $\mathbf{S}$ as indicated by the arrow. The quantitative results in Table 1 show that the SSIM and NRMSE values are significantly higher for the new approach. A SSIM could be increased from 0.81 for the best compared method to 0.94 for LoSDeCoS in the aorta. For the higher accelerated carotids the increase is even more evident, 0.82 instead of 0.65. The CNR_{VB} values for LoSDeCoS are superior to the compared as well as to the reference dataset, which is due to the higher suppression of background noise by exploiting the low rank. The CNR_{VT} was in the range of the reference, but lower than the compared methods. This result, combined with the significantly better SSIM and NRMSE, shows that LoSDeCoS preserves the vascular and tissue contrast better than the regularized SENSE method which tends to suppress the tissue more.

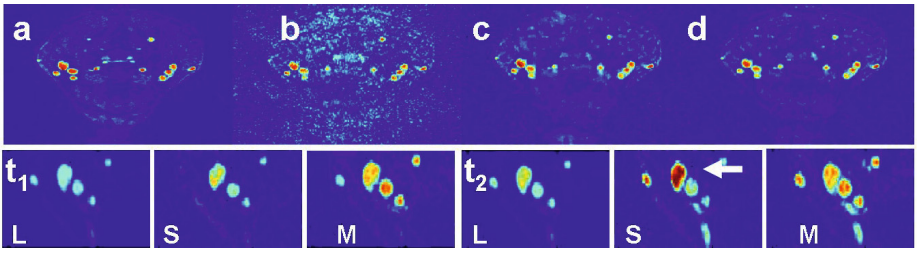

Fig. 3. Upper row: Carotid results for (a) reference, (b) IS, (c) IRS and (d) LoSDeCoS Lower row: Low-rank, sparse and combined result for phases t_1 and t_2

Table 1. Quantitative evaluation of the human data

	Aorta (acceleration 6.0)				**Carotids (acceleration 8.0)**			
	$\mathbf{X}_{REF}$	$\mathbf{X}_{IS}$	$\mathbf{X}_{IRS}$	$\mathbf{X}_{LOS}$	$\mathbf{X}_{REF}$	$\mathbf{X}_{IS}$	$\mathbf{X}_{IRS}$	$\mathbf{X}_{LOS}$
$SSIM$	1.00	0.79	0.81	0.94	1.00	0.30	0.65	0.82
$NRMSE$	0.00	118.51	115.63	93.84	0.00	183.91	144.29	138.50
CNR_{VT}	11.46	14.72	17.91	14.18	15.87	10.47	16.12	15.97
CNR_{VB}	26.27	14.03	16.32	27.06	24.14	11.83	22.10	29.25

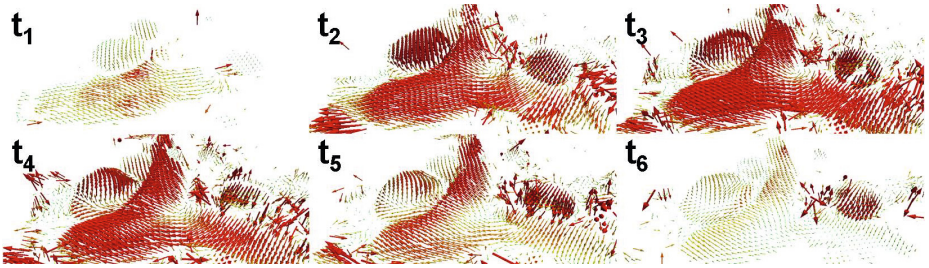

Fig. 4. Representation of the flow patterns in the aorta in 6 consecutive timesteps

In summary, the results show that LoSDeCoS achieves even at higher acceleration factors excellent results for the reconstructed volumes. The accuracy of this data is essential for the calculation of any meaningful physiological value calculation. Representative 3D velocity fields over time are shown in Fig. 4, the absolute flow values of the ascending aorta over the cardiac cycle obtained from the LoSDeCoS results (Fig. 5a) in comparison with the reference values illustrate that LoSDeCoS is very well suited to calculate accurate 4D flow results. A manual segmentation of the aorta done by an experienced radiologist was used to calculate the total flow F. Figure 5b,c illustrate the parabolic in-/outflow profiles obtained from phantom experiments using LoSDeCoS. The mass conservation deviation DM for LoSDeCoS equals 0.86%, compared to 4.5% for iterative regularized SENSE and 1.3% for iterative SENSE (Reference: 0.63%).

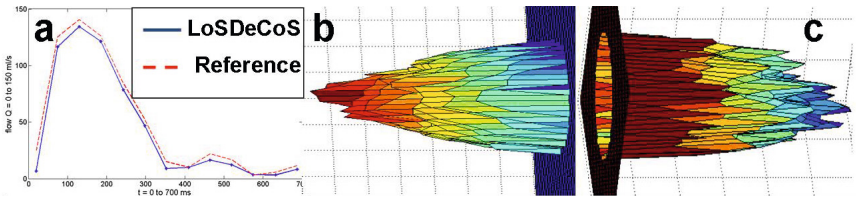

Fig. 5. (a) Aortic flow over time. (b-c) Parabolic In- and Outflow profiles

5 Discussion and Conclusions

The proposed LoSDeCoS algorithm has been proven to yield very good reconstruction results for 4D PCI data by enabling a significant reduction in acquisition time from roughly 10 min. for a 4D scan of the aortic arch down to under 2 min. While being successfully applied to both the carotid bifurcation region and the aortic arch, it has further shown its generalization capabilities to different body regions. In addition, the proposed reconstruction framework is, due to the splitting, well adapted to incorporate further regularizations such as phase corrections [13] or divergence terms.

Acknowledgements. The authors gratefully acknowledge funding of the Erlangen Graduate School in Advanced Optical Technologies (SAOT) by the German Research Foundation in the framework of the German excellence initiative.

References

1. Chai, P., Mohiaddin, R.: How we perform cardiovascular magnetic resonance flow assessment using phase-contrast velocity mapping. J. Cardiovasc. Magn. Reson. 7, 705–716 (2005)
2. Kim, D., Dyvorne, H.A., Otazo, R., Feng, L., Sodickson, D.K., Lee, V.S.: Accelerated phase-contrast cine MRI using k-t SPARSE-SENSE. Magn. Reson. Med. 67, 1054–1064 (2011)
3. Joseph, A.A., Merboldt, K.D., Voit, D., Zhang, S., Uecker, M., Lotz, J., Frahm, J.: Real-time phase-contrast MRI of cardiovascular blood flow using undersampled radial fast low-angle shot and nonlinear inverse reconstruction. NMR Biomed. 25, 917–924 (2011)
4. Tao, Y., Rilling, G., Davies, M., Marshall, I.: Compressed sensing reconstruction with retrospectively gated sampling patterns for velocity measurement of carotid blood flow. In: Proc. Joint Annual Meeting ISMRM- ESMRMB, Stockholm, Sweden, p. 4866 (2010)
5. Esser, E.: Applications of Lagrangian based alternating direction methods and connections to split Bregman. CAM Report 09-31, UCLA (2009)
6. Aelterman, J., Luong, H., Goossens, B., Piurica, A., Philips, W.: COMPASS: a Joint Framework for Parallel Imaging and Compressive Sensing in MRI. In: IEEE Int. Conf. on Image Processing (ICIP), Hong Kong, China, pp. 1653–1656 (2010)
7. Candes, E.J., Li, X., Ma, Y., Wright, J.: Robust principal component analysis? J. ACM 58, 11:1–11:37 (2011)
8. Majumdar, A., Ward, R.: Exploiting rank deficiency and transform domain sparsity for MR image reconstruction. Magn. Reson. Imaging. 30, 9–18 (2012)
9. Yin, X., Ng, B., Ramamohanarao, K., Baghai-Wadji, A., Abbott, D.: Exploiting sparsity and low-rank structure for the recovery of multi-slice breast MRIs with reduced sampling error. Med. Biol. Eng. Comput. (2012)
10. Tremoulheac, B., Atkinson, D., Arridge, S.R.: Motion and Contrast Enhancement Separation Model Reconstruction from Partial Measurements in Dynamic MRI. In (Proceedings) MICCAI Workshop on Sparsity Techniques in Medical Imaging, Nice, France (2012)
11. Goldstein, T., Osher, S.: The Split Bregman Method for L1-Regularized Problems. SIAM J. Img. Sci. 2, 323–343 (2009)
12. Wang, Z., Bovik, A.C., Sheikh, H.R., Simoncelli, E.P.: Image Quality Assessment: From Error Visibility to Structural Similarity. IEEE Transactions on Image Processing 13, 600–612 (2004)
13. Zhao, F., Noll, D.C., Nielsen, J.F., Fessler, J.A.: Separate Magnitude and Phase Regularization via Compressed Sensing. IEEE Trans. Med. Imaging 31, 1713–1723 (2012)